

Structures of chiral smectic-*C* mesophases revealed by polarization-analyzed resonant x-ray scattering

P. Mach,¹ R. Pindak,^{2,*} A.-M. Levelut,³ P. Barois,⁴ H. T. Nguyen,⁴ H. Baltes,^{2,†} M. Hird,⁵ K. Toyne,⁵ A. Seed,⁵ J. W. Goodby,⁵ C. C. Huang,¹ and L. Furenlid^{6,‡}

¹*School of Physics and Astronomy, University of Minnesota, Minneapolis, Minnesota 55455*

²*Bell Laboratories, Lucent Technologies, Murray Hill, New Jersey 07974*

³*Laboratoire de Physique des Solides, Université Paris–Sud, F-91405 Orsay, France*

⁴*Centre de Recherche Paul Pascal, CNRS, Université Bordeaux I, Avenue A. Schweitzer, F-33600 Pessac, France*

⁵*School of Chemistry, The University, Hull HU6 7RX, United Kingdom*

⁶*NLSL, Brookhaven National Laboratory, Upton, New York 11973*

(Received 22 February 1999)

We report polarization-analyzed, resonant x-ray diffraction at the sulfur K edge performed upon free-standing liquid-crystal films. Our studies of the thiobenzoate liquid-crystal enantiomer 10OTBBB1M7 yield the polarization states of resonant satellite peaks arising from characteristic superlattices in the chiral smectic-*C* (SmC^*) variant phases, including the antiferroelectric SmC_A^* , ferroelectric SmC_{F11}^* and SmC_{F12}^* , as well as SmC_α^* . The observed polarizations agree with the clock model of chiral smectic-*C* variants, and rule out other proposals made to date for these structures. Data from the 10OTBBB1M7 racemate also support the clock model. Our resonant diffraction results from a thiophene liquid-crystal compound reveal the same superlattice periodicities seen in corresponding antiferroelectric and ferroelectric phases of 10OTBBB1M7. [S1063-651X(99)12411-5]

PACS number(s): 61.30.Eb, 77.84.Nh, 78.70.Ck, 83.70.Jr

I. INTRODUCTION

The discovery in 1989 of the antiferroelectric, chiral smectic-*C* phase (SmC_A^*) in the MHPOBC liquid-crystal compound [1] sparked intense research effort to clarify the properties and origin of this novel structure. Although a ferroelectric, chiral smectic-*C* (SmC^*) structure for similar compounds containing chiral centers had already been proposed and detected [2] more than ten years earlier, finding strong antiferroelectric ordering within a liquid-crystal phase otherwise lacking truly long-range positional order was nonetheless surprising and very remarkable.

Many new materials have been synthesized over the past decade in an attempt to study the detailed structure of SmC_A^* and to determine the molecular characteristics which may promote its occurrence. One result of this work has been the identification of other SmC^* variants, including the so-called SmC_α^* and the *ferrielectric* phases SmC_{F11}^* and SmC_{F12}^* . As a function of decreasing temperature, a complete set of these phases would appear as SmC_α^* , SmC^* , SmC_{F12}^* , SmC_{F11}^* , and SmC_A^* [3]. The distinct electro-optic responses of these various phases, particularly SmC_A^* and SmC^* , have already led to important applications in optical switching devices with tristable properties [4–6], creating a great technological incentive for more experimental and theoretical work. A detailed understanding of the molecular ordering mechanisms

underlying the SmC^* variants also remains a fundamental goal of condensed-matter research. A successful theoretical model for the observed SmC^* phase sequences, supported by experimental data, should give important insight into the nature of the various intermolecular forces, such as steric, van der Waals, and electrostatic interactions, which can drive such a rich phase-transition series.

Many different experimental techniques have been applied to characterize the SmC^* variants' physical properties. Published reports include electro-optic [7,8], light scattering [9], birefringence [10], calorimetry [11,12], conoscopy [7,13], ellipsometry [14], optical observation [15], and x-ray studies [16,17]. The majority of these methods have not, however, been able to provide detailed pictures of the molecular orderings in the SmC^* variant phases [18]. In particular, conventional x-ray diffraction, usually a very powerful tool for obtaining direct information about molecular arrangements, fails to distinguish between the structures associated with the SmC^* variants. In a recent publication [19], we reported our successful application of resonant x-ray scattering to avoid this difficulty. Our data revealed distinct structural periodicities associated with the chiral SmC phases exhibited by one thiobenzoate liquid-crystal enantiomer compound (10OTBBB1M7) and the SmC_A phase of its racemic counterpart. We showed the existence of two-, three-, and four-layer superlattice periods in the SmC_A^* , SmC_{F11}^* , and SmC_{F12}^* phases, respectively, along with periodicity incommensurate with layer spacing in SmC_α^* . By comparing our results against several proposed models for the molecular arrangements, we showed that only the clock model [20] described the resonant x-ray peaks observed in all the variant SmC^* phases. Calculations of the tensorial structure factors appropriate for resonant x-ray scat-

*Author to whom correspondence should be addressed.

†Present address: Olympus Winter and Ibe GmbH, Kuehnstrasse 61, D-22045 Hamburg, Germany.

‡Present address: Dept. of Radiology, University of Arizona, Tucson, AZ 85724.

tering [21] have since provided distinct predictions for how diffracted x-ray polarization states would differ depending on the model used to describe the molecular structures. An experimental test of these polarization predictions was clearly an important and logical extension of our initial work.

In this paper, we report the recent enhancement of our experimental method to include polarization analysis of diffracted x rays. We have carried out an additional series of studies on the 10OTBBB1M7 enantiomer and racemate compounds, and determined the polarization state of the x rays contributing to each of the resonant diffraction peaks associated with the superlattices of the chiral SmC variants. We also performed a series of resonant-scattering measurements on a thiophene liquid-crystal compound (MHDDOPTCOB) exhibiting SmC* variants. These latter studies confirmed the ability of our technique to detect resonance signals originating from sulfur atoms in quite different chemical bonding environments. Importantly, the MHDDOPTCOB data also revealed the same superlattice periodicities observed in corresponding phases of 10OTBBB1M7.

In what follows, we first briefly review the nature of the mesophases studied and the sample geometry. We next describe our experimental arrangement and present the data obtained from two different liquid-crystal compounds. A comparison between our polarization results on 10OTBBB1M7 and the existing theory reveals complete agreement between our observations and the predictions of the clock model. Our results also rule out the so-called ‘‘Ising-like’’ model structures proposed in the past [3,22,23]. We indicate in our discussion some remaining issues to be resolved and our experimental plans to address them.

II. STRUCTURE OF THE CHIRAL SMECTIC-C PHASES STUDIED AND OUR SAMPLE GEOMETRY

The liquid-crystal molecules of interest are rod-shaped, ~ 40 Å in length and 5 Å in diameter. In the so-called smectic phases, these molecules organize to give a layered center-of-mass distribution, with well-defined orientational order accompanying the one-dimensional positional ordering. The smectic phases can thus be pictured as a stack of molecular layers, the positional order within any layer being purely liquidlike; at the same time, the molecules strongly tend to orient their long axes along a common direction known as the director, \mathbf{n} . The director is either along the layer normal \mathbf{z} (SmA phase) or is inclined with respect to the layer normal by some tilt angle β (SmC phases). Within the SmC phases, a projection (\mathbf{c}) of the molecular director \mathbf{n} onto the xy layer plane can be considered. The situation is shown in Fig. 1. The angle between \mathbf{c} and the x axis in the j th layer is denoted as Ψ_j and the change in Ψ_j between adjacent layers j and $(j+1)$ is $\Delta\Psi_j$. If the molecules are chiral, an overall helical rotation of \mathbf{c} develops with a pitch, P_0 , ~ 1 μm . The chiral

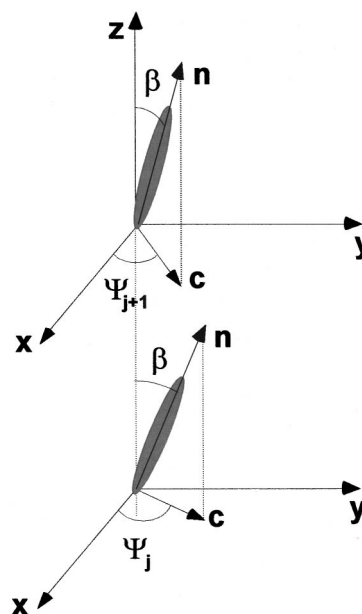


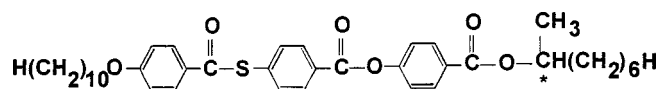
FIG. 1. Schematic diagram illustrating the orientation of molecules in neighboring SmC* layers. Tilt angle β in layers j and $(j+1)$ is the same, while azimuthal angles Ψ_j and Ψ_{j+1} differ: \mathbf{z} , \mathbf{n} , and \mathbf{c} are coplanar.

SmC phases are designated by SmC*. It is in the detailed progression of Ψ_j and $\Delta\Psi_j$ from layer to layer where proposed models of the molecular arrangements of the SmC* variants differ.

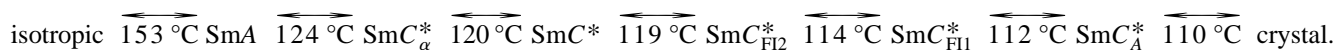
At appropriate smectic phase temperatures, many liquid-crystal compounds can form freely suspended films, similar to soap films supported on a ring. Such smectic films are created by simply pulling material from a bulk reservoir across an opening. The film thickness is quantized, restricted to an integer number of molecular layers; the layer normal coincides with the film normal direction.

In the x-ray work described here, the liquid-crystal compounds were studied in the free-standing film geometry. In contrast to typical bulk sample cell preparations, the free-standing film provides a well-defined, uniform orientation of the smectic layers without requiring any extra aligning surface that would in turn attenuate the x-ray intensity. In our experiment, the x rays are incident onto the film in the Bragg geometry.

The material studied in our polarized x-ray-scattering experiment was 10OTBBB1M7 [24], which has the following structure:



The bulk 10OTBBB1M7 enantiomer shows the following phase sequence:



A critical feature of 10OTBBB1M7 for the purposes of our experiment is the sulfur atom contained within the center portion of the molecule. Conventional x-ray diffraction along the Q_z reciprocal space direction probes the in-plane-averaged electron density. All of the SmC^* variants give Q_z peaks only at integral multiples of $Q_0 = 2\pi/d$, where d is the smectic layer spacing. Therefore, the z -projected electron density is identical for all of the variants, and they differ from one another only by symmetry elements such as glide planes or screw axes along \mathbf{z} . By working with x rays whose energy is at the sulfur's K absorption edge, the structure factor becomes a tensor instead of the conventional scalar [21,25]. The scattered x-ray intensity now varies depending on the molecular orientation, since the off-diagonal tensor components depend on the orientation of the bonds around the sulfur atom with respect to the polarization of the incident x-ray beam [26]. Because $\Delta\Psi_j$ arrangements of various SmC^* subphases are distinct, under this circumstance the resonant x-ray diffraction is capable of revealing the structural differences.

III. EXPERIMENTAL DESCRIPTION

Our x-ray studies were performed at beamline X-19A of the National Synchrotron Light Source (NSLS) at Brookhaven National Laboratory. The central component of our experimental setup is a sample chamber designed to hold the liquid-crystal compounds at the appropriate elevated temperatures. The inner portion of the chamber is a two-stage oven containing a stainless-steel film plate. The freely suspended films were spread across a 1-cm-diam, knife-edged circular hole in this plate. The film temperature was monitored by a type- E thermocouple mounted on the plate directly at the film's edge.

The two-stage oven is enclosed by an outer aluminum can. X-ray access to the film is provided by apertures in the various side walls. Windows in the top plates of the outer can and oven enabled us to visually estimate the thicknesses of the films we spread [27]. We were able to monitor the films' thickness and phase uniformity over time by using a long working distance microscope with an attached CCD camera. The sample was illuminated from the top with polarized light, and light specularly reflected from the film passed through a slightly uncrossed analyzer before entering the camera/microscope assembly. Under these viewing conditions, the inherent birefringence of the liquid-crystal molecules gives rise to characteristic optical textures. During x-ray measurements on a given film, we found that this ability to simultaneously monitor the optical texture was quite important, since it enabled us to observe the onset of transitions between various SmC^* phases. In addition, we were able to recognize conditions such as two-phase coexistence and avoid data collection under such questionable circumstances.

The elements of our x-ray flight path are described as follows. Upon exiting from beamline vacuum through an 8- μm beryllium window, the x rays first pass through an adjustable slit assembly that defines the dimensions of the incident beam to 0.5 mm vertical by 1.0 mm horizontal. After exiting the slits, the x-ray beam then passes through an in-line ionization monitor before finally entering the sample

chamber. The signal from this in-line monitor was used to normalize out any drift in the beam intensity incident upon our films. Additionally, the upstream flight path contains a unit allowing a powder liquid-crystal sample to be translated into or out of the x-ray beam. A detector attached to this assembly at a 90° orientation to the beam path collects fluorescent radiation from the powder. The beamline optics at line X-19A include a collimating mirror, a double flat crystal Si(111) monochromator, and a toroidal (bent cylinder) focusing mirror. We are therefore able to sensitively vary incident x-ray energy and monitor the corresponding fluorescence signal. We use the principal maximum of such a fluorescence intensity curve to determine the sulfur's K -edge resonant energy. This energy has been found to be 2475 eV for the sulfur atom in both materials studied.

The x rays diffracted from the film, after exiting the oven, travel down an approximately 1.1-m-long flight tube, before entering the polarimeter assembly. The first element of the polarimeter is a 0.5 mm, resolution-setting circular aperture, mounted on the center of rotation of a motorized stage. The rotation axis of this analyzer χ_a stage is carefully aligned to coincide with the diffracted x-ray beam's direction of travel. The x rays are subsequently incident upon a pyrolytic graphite (PG) crystal contained inside the body of the polarimeter assembly. The angle of the x rays upon the crystal face, denoted here as the analyzer crystal angle θ_a , is adjusted to match the Bragg angle for PG at the resonant x-ray energy. The x rays diffracted from the PG crystal pass through a thin Mylar foil window in the polarimeter assembly wall, and are detected on the outside by a neon-filled proportional counter. Our system can also be used to acquire simple Q_z scans without polarization analysis by translating the PG crystal out of the beam path and repositioning the proportional counter onto the end of the detector arm assembly.

The principle behind our polarimeter design is straightforward. Rotating the pyrolytic graphite crystal about the χ_a axis, while keeping the incidence angle, θ_a , fixed to the Bragg angle, modulates the intensity diffracted from the crystal in a manner depending on the incident x rays' polarization. For linearly polarized x rays, the intensity profile observed as a function of χ_a can be shown to vary as $\sin^2(\chi_a)$. The ideal case, with diffracted intensity modulated completely to zero, can only occur when the Bragg angle for the analyzer crystal equals 45°. This was a primary reason for choosing pyrolytic graphite as our analyzer crystal material, since the Bragg angle at 2.475 keV is approximately 48.3°. This value is quite close to 45°, and means that the diffracted intensity, as a function of χ_a , will have a minimum-to-maximum intensity ratio of only a few percent. Thus, when analyzed by our polarimeter assembly, σ -polarized x rays (σ defined here as a unit vector in the plane of the synchrotron ring) give a characteristic $\sin^2(\chi_a)$ profile 90° offset in a χ_a coordinate from the π -polarized case. This ability to distinguish σ versus π polarization is a critical feature of our experiment. For example, the tensorial structure factor calculations carried out based upon the clock model for the SmC^* variants [21] specifically predict diffraction of incident σ into outgoing π polarization for certain orders of satellite reflections from the structural superlattice periodicities. The combination of highly σ -polarized incident x-ray radiation available at the synchrotron beam-

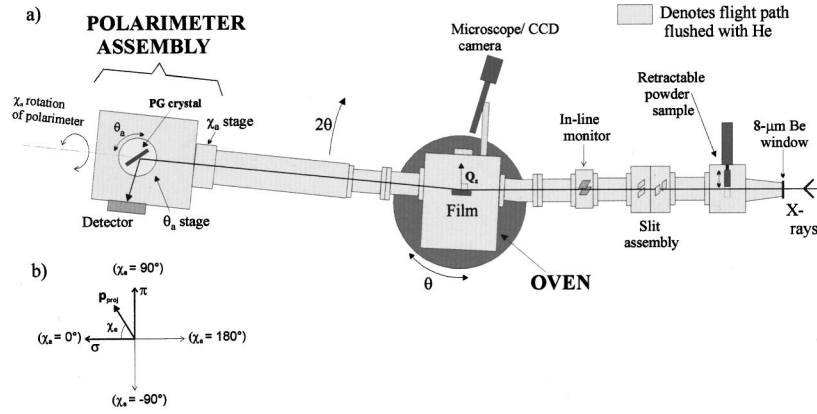


FIG. 2. (a) Schematic diagram of components in the polarized resonant x-ray-scattering experiment. (b) Coordinates relevant to the polarimeter unit in our study. \mathbf{p}_{proj} is the projection of a unit vector normal to the PG crystal surface, and within the incidence plane, onto the plane defined by the σ and π polarization unit vectors.

line, together with diffracted x-ray polarization analysis, enabled us to conclusively test the model's predictions.

We should emphasize that all components of our x-ray setup, from the beryllium beamline exit window up to, and including, the enclosed polarimeter assembly, were connected together with flight tubes so as to maintain a sealed beam path. During the course of our measurements, this flight path was kept flushed with helium gas. Operation in a helium environment was essential to our experiment in order to avoid the prohibitive reduction in intensity that would otherwise occur due to air absorption at 2.5 keV.

The film oven, and all of the components comprising the detection “arm” of our assembly, are mounted on the θ and 2θ circles, respectively, of a Huber two-circle goniometer. An overall schematic view of our x-ray setup incorporating polarization analysis is given in Fig. 2.

IV. DATA

In Figs. 3–5, we give the results of our Q_z/Q_0 scans on the MHDDOPTCOB compound. The bulk phase sequence of this material is



The molecular structure is given in Fig. 3, which also shows a series of Q_z/Q_0 scans performed in the SmC^* phase at different x-ray energies near sulfur resonance (E_0) of 2.475 keV [29]. The x-ray signature shows satellite peaks closely spaced about the conventional second-order Bragg reflection; no peaks at any other nonintegral Q_z/Q_0 are seen. For $|E - E_0| \geq 5$ eV, these satellites about the conventional Bragg reflection disappear, confirming their resonant-scattering origin. Figure 4 shows data collected in the ferroelectric phase of MHDDOPTCOB. The resonance peaks located at quarter-integer Q_z/Q_0 indicate that the phase identification should be SmC_{FI}^* [28], corresponding with the four-layer superlattice periodicity. Figure 5 gives data from the MHDDOPTCOB SmC_A^* phase; the two-layer superlattice is indicated by the half-order resonant peak structure. We interpret the features visible in Figs. 3–5 in our discussion below, noting for now that they are consistent with the expectations based on prior 10OTBBB1M7 results, and agree with the predictions of the clock model.

Our subsequent studies on the 10OTBBB1M7 R-enantiomer and racemate compounds focused on the polarization analysis of the resonant diffraction peaks. Consequently, we needed to confirm our polarimeter's ability to resolve the highly σ -polarized nature of x rays supplied by the X-19A beamline. For this characterization, we set the x-ray energy to 2613.9 eV, where the Bragg angle for the PG crystal is exactly 45° . A χ_a orientation of $\pm 90^\circ$ corre-

sponded to a PG crystal incidence plane oriented perpendicular to σ , with the x-ray beam being diffracted vertically. $\chi_a = 0^\circ$ or 180° orientations corresponded to a horizontal PG crystal diffraction plane, containing σ . The $\chi_a = \pm 90^\circ$ cases should therefore give intensity maxima for incident σ polarization.

Figure 6 gives the observed diffracted intensity curve obtained over a full 360° rotation in χ_a for a 2613.9 eV x-ray beam traveling through the complete experimental beam path, but without diffracting off a liquid-crystal film. The fit supplied in Fig. 6 is the expected sine-squared functionality, allowing for a background level (comprised of either genuine π - or simply unresolved-polarization intensity) and a phase angle χ_0 . Overall, a very good fitting agreement is obtained, with parameters corresponding to a negligible background signal and only a very small χ_0 offset. We should note that while the maxima of the observed curve fall at the expected $\pm 90^\circ$ positions, there is a skewing of the overall profile resulting in higher intensity at -90° and lower diffraction intensity at $+90^\circ$. This additional intensity modulation of the sine-squared behavior was a consistent feature of our χ_a scans; we attribute such a systematic effect to a geometric feature of our setup. Namely, at $\chi_a = -90^\circ$, the PG crystal is in a nondispersive orientation with respect to the second crystal of the beamline monochromator, whereas at $\chi_a = +90^\circ$, the PG crystal is in a dispersive geometry. These dispersive/nondispersive considerations did not, however, di-

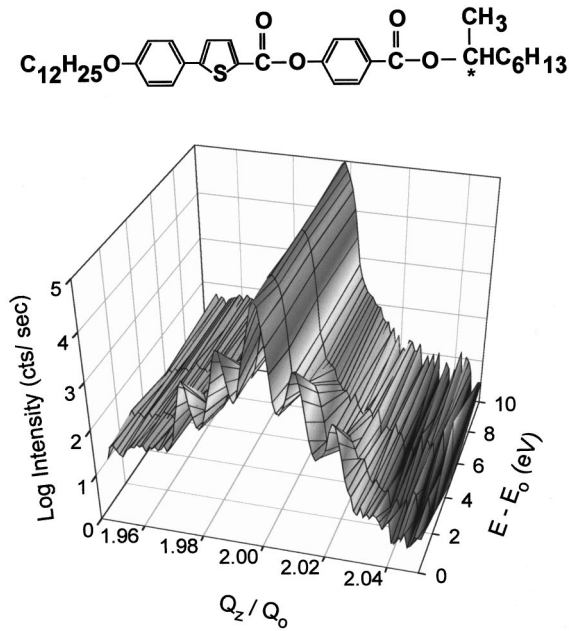


FIG. 3. X-ray intensity scans in the SmC^* phase of the MHDDOPTCOB as a function of incident beam energy relative to the sulfur K -edge absorption maximum. Shown above is the MHDDOPTCOB molecular structure.

minish our ability to distinguish σ and π polarizations, as is evident from our data. The minimum- to maximum-observed intensity ratio in Fig. 6 is approximately 3×10^{-4} , together with $\chi_0 = 1^\circ$, giving us a high degree of confidence in the performance of our polarimeter, while at the same time confirming the incident beam's sigma polarization.

Once we had performed the initial polarimeter/x-ray beam analysis, we sought to establish the polarization state of x rays contributing to the resonance peaks characterizing the SmC^* variant phases. To observe these peaks, we worked at the previously determined 10OTBBB1M7 sulfur resonance energy of 2.475 keV [19]. As a check, we first performed polarization analysis on the $Q_z = 2Q_0$ Bragg peak from a 10OTBBB1M7 film in the SmC_A^* phase. The diffracted ra-

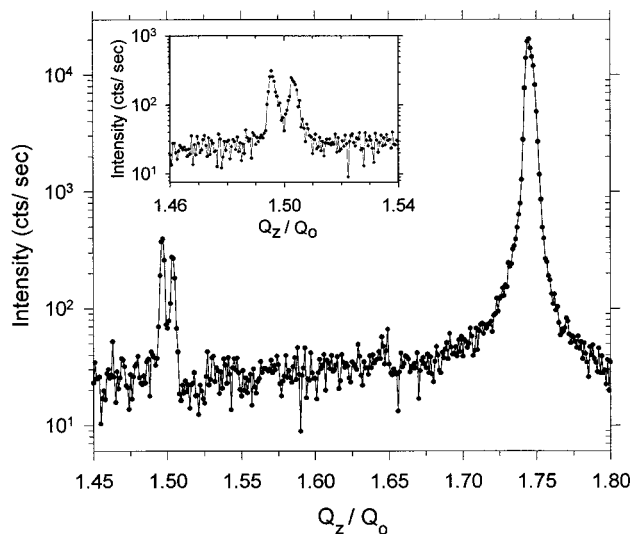


FIG. 4. X-ray intensity scan in the ferrielectric phase (identified as SmC_{F12}^*) of MHDDOPTCOB.

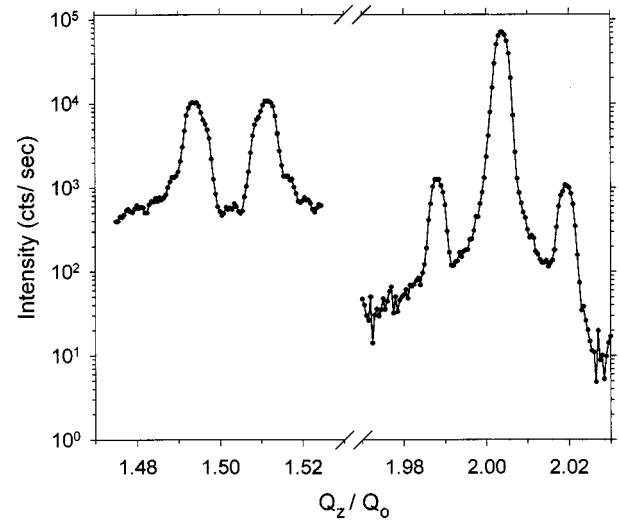


FIG. 5. X-ray intensity scan in the SmC_A^* phase of MHDDOPTCOB. Splitting of the first-order resonant satellite peaks about $1.5 Q_0$, and the second-order resonant satellites on either side of the conventional Bragg peak, are shown.

diation observed at this Q_z value should be dominated by conventional x-ray scattering, and no alteration of the incident polarization state is therefore expected. Our polarization data on the $2Q_0$ peak were in complete agreement with these expectations, allowing us to proceed to the next stage of our measurements.

In the remaining presentation of our data, we focus on the resonant-scattering peaks [30] observed for both R-enantiomer and racemic 10OTBBB1M7 [31]. In Figs. 7(a) and 7(b) we show data taken on 10OTBBB1M7 in the SmC_A^* phase. Figure 7(a) gives integrated peak intensities as a function of χ_a for the lower of the two peaks centered about $1.5Q_0$. Figure 7(b) presents corresponding data for the upper peak. The inset to Fig. 7(a) shows the overall appearance of these resolution-limited peaks in a typical Q_z scan performed

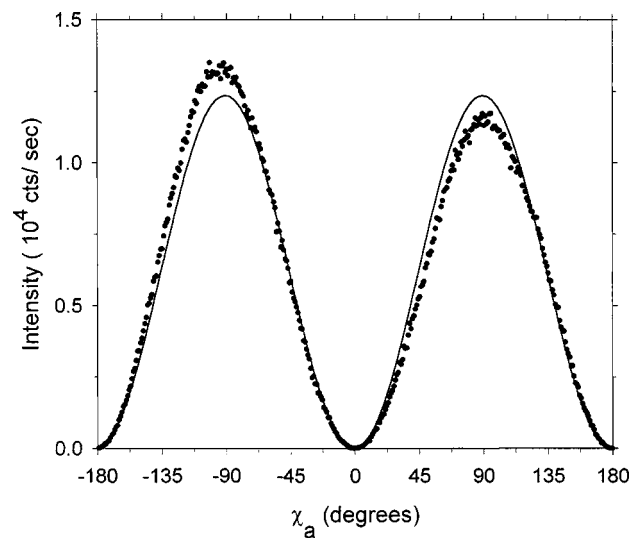


FIG. 6. Observed intensity vs χ_a orientation for 2613.9 eV x rays from NLS beamline X-19A analyzed by our polarimeter. The solid line is a fit to $I_0 + A \sin^2(\chi_a + \chi_0)$, yielding $I_0 = 0$, $A = 1.23$, $\chi_0 = 0.99$. In our coordinate system, a $\chi_0 \approx 0$ implies σ polarization.

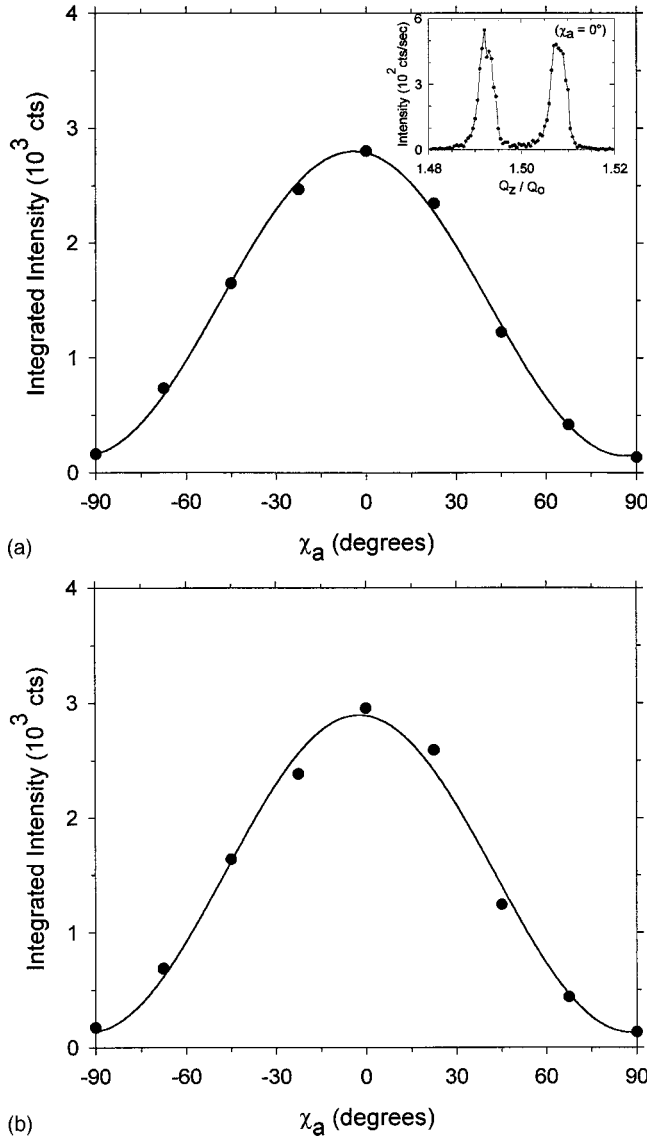


FIG. 7. Intensities integrated from Q_z/Q_0 scans of the first-order resonant satellites in the SmC_A^* phase of 100TBBB1M7, as a function of PG analyzer crystal orientation. The centers for these satellite peaks were at $1.492Q_0$ (a) and $1.508Q_0$ (b). The solid lines for the integrated intensity data are fits to $I_0 + A \sin^2(\chi_a + \chi_0)$, yielding $I_0 = 0.15$, $A = 2.65$, $\chi_0 = 94.0$; and $I_0 = 0.13$, $A = 2.76$, $\chi_0 = 92.2$, respectively, for (a) and (b). A $\chi_0 \approx 90$ implies π polarization.

at a fixed $\chi_a = 0^\circ$ [32]. Such a splitting structure observed at half-integer Q_0 value is characteristic of the two-layer antiferroelectric superlattice in SmC_A^* , coupled to a long helical pitch [19], as discussed below in the context of the clock model. The maxima of both Figs. 7(a) and 7(b) are offset by approximately 90° from the corresponding features in the previous incident beam and $2Q_0$ peak scans. The data therefore show the π -polarized nature of the SmC_A^* superlattice peaks.

Clear indications of the diffracted radiation's polarization were also obtained for the characteristic resonant peaks in the ferroelectric and SmC_α^* phases of 100TBBB1M7. Figure 8 shows representative data taken in the $\text{SmC}_{\text{FI2}}^*$ phase. π polarization for the $1.25Q_0$ and $1.75Q_0$ peaks is shown in

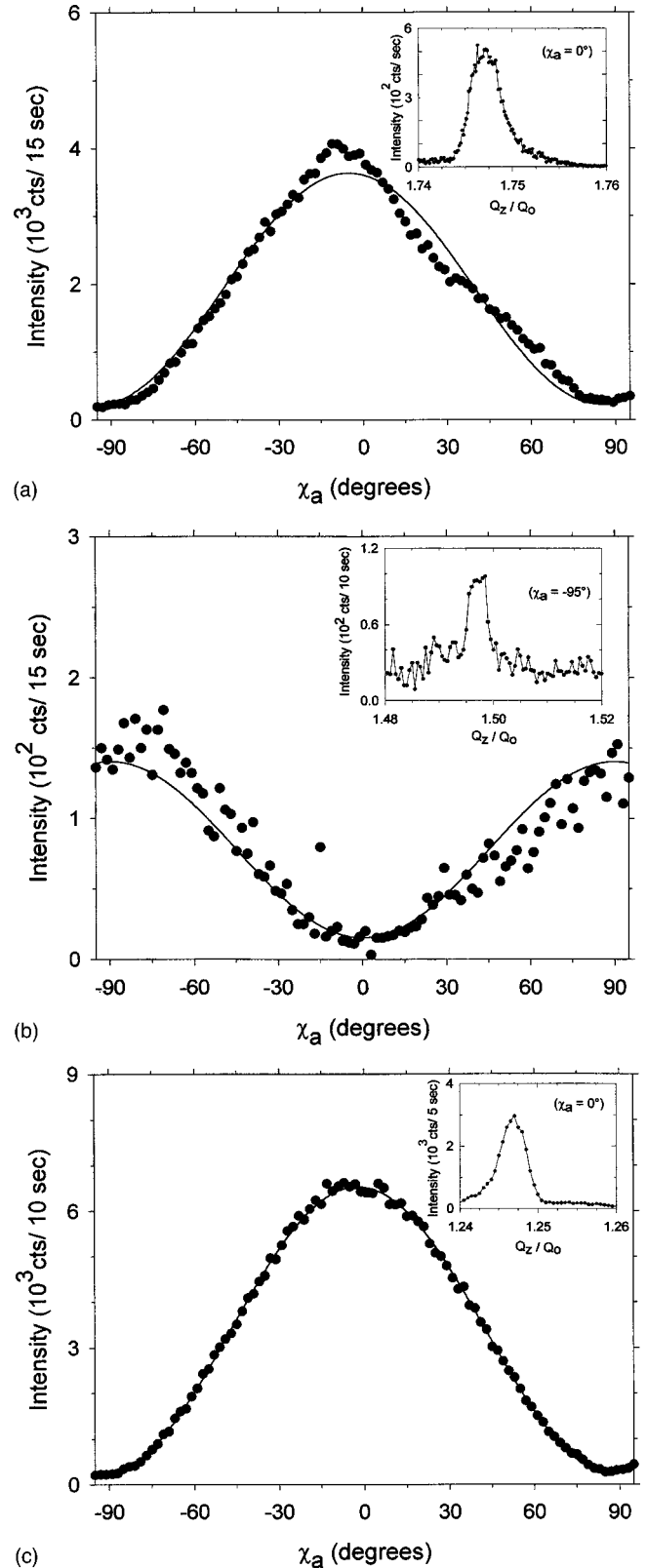


FIG. 8. Intensities as a function of PG analyzer crystal orientation, for scattering wave-vector values set to (a) $1.746Q_0$; (b) $1.497Q_0$; (c) $1.247Q_0$ in the $\text{SmC}_{\text{FI2}}^*$ phase of 100TBBB1M7. The solid lines in (a) and (c) are fits to $I_0 + A \sin^2(\chi_a + \chi_0)$, yielding parameters (a) $I_0 = 0.22$, $A = 3.41$, $\chi_0 = 95.1$; (c) $I_0 = 0.24$, $A = 6.29$, $\chi_0 = 92.3$. The fit in (b) is to $I_0 + A \sin^2(\chi_a)$, yielding $I_0 = 0.15$, $A = 1.25$. Insets show corresponding resonant satellite peaks in simple Q_z scans.

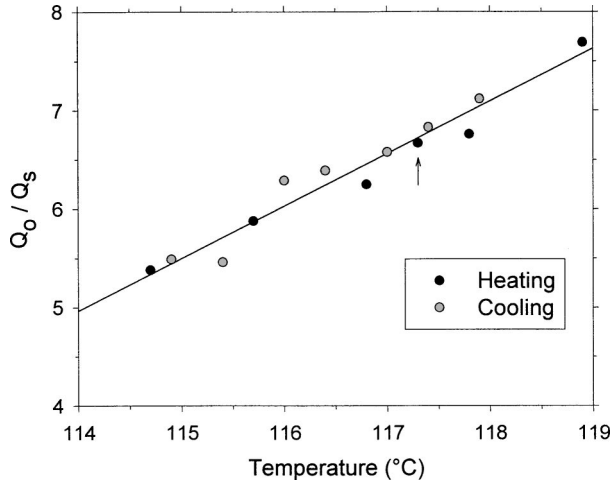


FIG. 9. Structural ratio Q_0/Q_s , Q_s the nonintegral component of resonant satellite position in the SmC_α^* phase of 10OTBBB1M7. The arrow indicates a data point inserted for comparison from the most recent experiment; the remaining data points were recorded in our previous work [19].

Figs. 8(a) and 8(c). The corresponding insets are Q_z scans performed at χ_a values chosen to maximize detected intensity; the peaks are nearly resolution-limited. Figure 8(b) shows analogous data for the $1.5Q_0$ peak of $\text{SmC}_{\text{FI}2}^*$, although in this case the polarization is sigma [33].

We also measured the polarization state of the $\text{SmC}_{\text{FI}1}^*$ resonant peaks in 10OTBBB1M7. Polarization analysis was done at a fixed $Q_z = 1.67Q_0$, corresponding to the principal maximum of the resonance peak we saw in this phase, agreeing once again with the three-layer superlattice we reported earlier [19]. The observed intensity versus χ_a profile confirmed a π polarization. Our improved Q_z resolution in these most recent measurements allowed us to resolve a fine substructure within the $\text{SmC}_{\text{FI}1}^*$ resonance peak. A more careful exploration of this substructure origin is a priority for our future studies of $\text{SmC}_{\text{FI}1}^*$.

Our previous work [19] revealed that the SmC_α^* phase in 10OTBBB1M7 is characterized by resonant-scattering peaks which imply the presence of a superlattice incommensurate with the smectic layer spacing. A distinct temperature dependence to this superlattice periodicity was observed, evolving from approximately eight layers at the upper end of the SmC_α^* window to five layers just above the observed transition to the $\text{SmC}_{\text{FI}2}^*$ phase [34]. This evolution can be seen in Fig. 9, where we plot as a function of film temperature the ratio Q_0/Q_s , Q_s being the nonintegral component of the SmC_α^* satellite peak position. In the course of the experiment reported here, we again observed such behavior. We carried out polarization analysis on a representative, resonant satellite peak centered at $1.15Q_0$ for a film temperature within the SmC_α^* window. The results obtained clearly indicate a π polarization, the profile of intensity versus χ_a exhibiting the characteristic sine-squared maximum at $\chi_a = 0^\circ$.

We were also able to study an approximately 250-layer-thick film of the racemic 10OTBBB1M7 compound. We performed polarization analysis on the $1.5Q_0$ resonant peak in the SmC_A phase. In this case, because there is no optical pitch, the resonant peak is unsplit. However, just as for the

SmC_A^* analogs shown in Fig. 7, the SmC_A resonance peak was clearly observed to be π -polarized.

V. DISCUSSION

Many different models have been proposed to explain the molecular arrangements within the SmC^* -like phases. Each of these theories can incorporate superlattice periodicities, i.e., allow for a periodic variation of the molecular orientation Ψ_j throughout the smectic layers. It is such an orientational superlattice that the resonant x-ray-scattering process can detect, and for which our initial 10OTBBB1M7 results [19] provided clear evidence.

For a given Ψ_j periodicity of ν layers, the theoretical models differ in the details of the Ψ_j and $\Delta\Psi_j$ progressions. For example, neglecting for the moment the effects of the long-wavelength optical pitch $P_0 \gg d$, in the so-called Ising models [3,22,23], Ψ_j orientations are restricted to a plane, and therefore only $\Delta\Psi_j$ values of 0 or π are possible. To our knowledge, there exist two somewhat different Ising models: one model developed to explain SmC^* variant sequences observed as a function of temperature [22], and the second model arising from studies of phase transitions under applied electric fields [23]. We will refer to the former model as the “ T Ising model” and the latter as the “ E Ising model.” For $\nu > 3$ layers, the T and E Ising models give explicitly different Ψ_j and $\Delta\Psi_j$ patterns. A detailed discussion of the predicted Ψ_j and $\Delta\Psi_j$ sequences has been given elsewhere [3,21].

Other competing models for the SmC^* variants include a bilayer model [35] and a model proposing a clocklike interlayer rotation of the molecular tilt direction [20], which we will refer to as the “clock model.” The bilayer model proposes a fundamental $\nu=2$ periodicity as an element of all SmC^* variants. Because we see clear evidence in the different 10OTBBB1M7 phases for $\nu=2,3,4$, or even noninteger value, the bilayer approach clearly could not describe the full range of SmC^* variants, and is therefore ruled out as a model of general validity. The clock model, on the other hand, does not restrict ν , and, unlike the Ising model, allows Ψ_j and $\Delta\Psi_j$ to assume all values from 0 to 2π . Specifically, for a ν -layer superlattice, the clock model specifies a helical progression of Ψ_j from layer to layer, with a fixed $\Delta\Psi_j = \Delta\Psi_0 = 2\pi/\nu$. Including the effect of the optical pitch, P_0 , $\Delta\Psi_0 = 2\pi/\nu + 2\pi d/P_0 = 2\pi[(1/\nu) + \varepsilon]$, where $\varepsilon = d/P_0$. The resultant helix rotates through 2π after $[(1/\nu) + \varepsilon]^{-1}$ layers, and hence has a pitch $P_H = d[(1/\nu) + \varepsilon]^{-1}$ and associated wave vector $Q_H = 2\pi/P_H = 2\pi[(1/\nu) + \varepsilon]/d = Q_0[(1/\nu) + \varepsilon]$.

Detailed calculations of resonant-scattering tensorial structure factors for the Ising and clock models of various ν have been carried out [21]. We note here a general result for the clock model. Namely, for a ν -layer superlattice periodicity, resonant-scattering peaks are expected at Q_z values of $Q_z = lQ_0 + mQ_H$ or

$$Q_z/Q_0 = l + m[(1/\nu) + \varepsilon]. \quad (1)$$

Here l and m are integers. Specifically, $l=0,1,2,\dots$; $m=0, \pm 1$, and ± 2 , where the five values for m result from the five independent components of the x-ray susceptibility ten-

sor [21]. This result indicates that resonant-scattering peaks should be expected to occur as first- and second-order satellites about integral Q_z/Q_0 peak positions.

As discussed in our previous publication [19], the observed Q_z coordinates of our resonant peaks for 10OTBBB1M7 can be well interpreted in the context of this clock-model result. Here we adopt the convention of labeling the observed peaks by the notation (h, k, l, m) , where h , k , and l are the usual reciprocal space indices corresponding to momentum transfer in the x , y , and z directions, respectively. Also, m refers to the resonant satellite peak order, and appears together with l in Eq. (1) above. Since our scans probed Q_z periodicity only, $h=0$ and $k=0$ for all cases. Consequently, our peak notation further simplifies to two distinct indices (l, m) . As a concrete example, consider the SmC_A^* phase, in which the resolution-limited peaks that split about $Q_z/Q_0=1.5$ (Fig. 7) correspond to the pair of peaks (1,1) and (2,-1). Inserting this (l, m) assignment into Eq. (1) yields $\nu=2$ and $\epsilon=0.008$, in other words, a two-layer superlattice periodicity coupled to a much longer optical pitch of approximately 4800 \AA (here we have inserted the measured layer spacing $d=38.2 \text{ \AA}$) [36]. Similarly, in the $\text{SmC}_{\text{F12}}^*$ phase, the resolution-limited (1,1) peak seen at $Q_z/Q_0=1.25$, the (1,2) and (2,-2) peaks at $Q_z/Q_0=1.50$, and the (2,-1) peak at $Q_z/Q_0=1.75$ imply a four-layer superlattice; the lack of observed splitting implies an ϵ smaller than our resolution, or equivalently a P_0 greater than approximately $2.5 \mu\text{m}$, based on the known width of our system resolution function [32]. Likewise, the one-third integer resonant peaks of $\text{SmC}_{\text{F11}}^*$ imply a three-layer superlattice periodicity ($\nu=3$), while the SmC_α^* resonance peak positions indicate an incommensurate superlattice.

The observed resonant peak positions in MHDDOPTCOB are in agreement with those of the 10OTBBB1M7 enantiomer for corresponding phases. For example, the peaks observed in Fig. 3 on either side of the conventional Bragg reflection in MHDDOPTCOB's SmC^* phase are (in ascending order) the (2,-2), (2,-1), (2,1), and (2,2) resonant satellite peaks of the SmC^* phase [37]. The ferroelectric phase of MHDDOPTCOB yields peaks at quarter-integer Q_z/Q_0 , just as for the $\text{SmC}_{\text{F12}}^*$ phase of 10OTBBB1M7. The different optical pitch value in MHDDOPTCOB leads to an observable splitting of the second-order $\nu=4$ satellites; this can be seen in the inset of Fig. 4, which shows distinct (1,2) and (2,-2) peaks of $\text{SmC}_{\text{F12}}^*$, implying a $P_0 \approx 2.3 \mu\text{m}$. Figure 5 indicates for MHDDOPTCOB's SmC_A^* window the same split-peak structure about half-integer Q_z/Q_0 observed for the corresponding phase in 10OTBBB1M7. Via Eq. (1), a splitting about the half-order position by $\epsilon=0.0085Q_0$ implies that second-order (1,2) and (3,-2) peaks should show $2\epsilon=0.017Q_0$ splitting, which is indeed seen in Fig. 5. In the case of MHDDOPTCOB, we are able to see the second-order resonant satellites, which are unresolved within the shoulders of the conventional $2Q_0$ peak in 10OTBBB1M7. The more rigid bonding environment of the sulfur in MHDDOPTCOB may be responsible for the enhanced higher-order resonance signal.

The resonance peak Q_z positions are valuable in and of themselves for testing the validity of the proposed SmC^* variant models. While entirely consistent with the clock-

model predictions, our results enable us to immediately rule out the T Ising model in the case $\nu=4$. Namely, the $\Delta\Psi_j = 0, \pi, 0, \pi$ repeating pattern leads to an *absence* of resonant peaks at half-integer Q_z/Q_0 [21]. In contrast, we observed (for both enantiomer compounds studied) resonant peaks at such positions in the $\text{SmC}_{\text{F12}}^*$ phase [19].

Importantly, the tensor structure factor calculations [21] make unambiguous predictions for the polarization state of radiation diffracted at the characteristic resonance peak positions. Specifically, the first-order resonant satellites ($m = \pm 1$) of the clock model are expected to scatter incident σ into outgoing π polarization. We have confirmed precisely such a result for the corresponding peaks. In 10OTBBB1M7 R-enantiomer, this behavior holds for the (1,1) and (2,-1) peaks in SmC_A^* ($Q_z/Q_0=1.492$ and 1.508 , respectively, shown in Fig. 7), for (1,1) and (2,-1) peaks in $\text{SmC}_{\text{F12}}^*$ [$Q_z/Q_0=1.25$ and 1.75 , respectively, shown in Figs. 8(a) and 8(c)], for the (2,-1) peak in $\text{SmC}_{\text{F11}}^*$ ($Q_z/Q_0=1.67$), and for the (1,1) peak in SmC_α^* (e.g., $Q_z/Q_0=1.15$). The same polarization behavior is expected for the racemic compound. We have confirmed this prediction as well by measuring π polarization for the (1,1) [equivalently (2,-1)] peak position in SmC_A ($Q_z/Q_0=1.50$). We should note that the E Ising model for these phases also yields π polarization for the first-order resonant satellite peaks. However, the E Ising and clock models differ greatly in their prediction of the polarization state for the $m = \pm 2$ peaks. We must consider next our observed polarization results with specific attention to this difference between the two competing models.

The second-order resonant satellites are expected under the clock model to preserve the incident σ polarization in the diffracted beam. Our results are in agreement with this prediction, too, as can be seen by the σ polarization of the (1,2) [equivalently (2,-2)] peak position in $\text{SmC}_{\text{F12}}^*$ [$Q_z/Q_0=1.50$, shown in Fig. 8(b)]. Actually, conversion of σ to π intensity is possible in principle within the second-order resonant satellites, but this contribution will be reduced by a $\sin^2(\theta)$ factor relative to the σ polarization-preserving term. For our range of film Bragg angles, $\theta=4^\circ$ to 7.5° , this contribution should be quite small. We also note for completeness that a truly commensurate three-layer superlattice period in $\text{SmC}_{\text{F11}}^*$ implies that the first-order (2,-1) satellite at $Q_z/Q_0=1.67$ is equivalent in Q_z position to the second-order (1,2) satellite. Consequently, a slightly enhanced σ -polarized component to the diffracted intensity measured at this position might be expected. Nonetheless, the strongly π -polarized character we observed for the $\text{SmC}_{\text{F11}}^*$ peak is consistent with the clock-model predictions for this structure.

The polarization analysis carried out on the resonance peaks is not only in agreement with the clock-model predictions, but also contradicts the expected polarization behavior derived from the E Ising model. Namely, in the $\nu=4$ E Ising case, the second-order satellites [(1,2) or (2,-2) position] are expected to have the same polarization as their first-order counterparts [i.e., (1,1) and (2,-1)] [21]. The clear π versus σ polarization difference we observe between the first- and second-order resonant satellites in $\text{SmC}_{\text{F12}}^*$ (Fig. 8) means that the E Ising description cannot adequately describe this phase; consequently, we can rule out E Ising as a model of general validity for the complete SmC^* variant series.

Our 10OTBBB1M7 results also suggest important directions for future experiments. While the clock model offers an excellent account for all our polarized x-ray-scattering data, it seems that the commensurate ($\nu \leq 4$) clock structure of the ferrielectric phases should exhibit uniaxial optical properties in a sufficiently thick sample. This is in contrast to the biaxiality required to explain the reported electro-optical behavior of the ferrielectric phases [3,13]. This discrepancy indicates that a distorted clock model may be required to successfully explain both the x-ray and optical measurements [21]. In our future studies, we plan to observe the resonance peak signatures of these phases as a function of an aligning electric field applied to the free-standing films. Such measurements should help us resolve the above-stated discrepancy. Second, the evolution of satellite peaks found in the 10OTBBB1M7 compound suggests that the commensurate clock picture ‘ends’ at $\nu = 4$, while for $\nu > 4$ an incommensurate arrangement is favored, as found in the SmC_α^* phase. Thus, the SmC_α^* phase seems to be a natural extension of the $\text{SmC}_{\text{F12}}^*$ phase. Polarized resonant scattering studies on other suitable compounds should help confirm whether this scenario is always the case for chiral compounds exhibiting the SmC^* variants. Additional questions that should be answered include whether the commensurate clock structure has a fundamental limit to $\nu \leq 4$, and why the SmC^* phase can appear between the more tightly wound SmC_α^* and $\text{SmC}_{\text{F12}}^*$ in certain materials.

VI. SUMMARY

We have performed the first resonant x-ray-scattering measurements upon the SmC_A^* , $\text{SmC}_{\text{F11}}^*$, $\text{SmC}_{\text{F12}}^*$, and SmC_α^* liquid-crystal phases with incorporated polarization analysis of the diffraction peaks. By working at the K -edge energy for sulfur atoms contained in the liquid-crystal molecules, the degeneracy of the SmC^* variants with respect to conventional Q_z x-ray scans is lifted. The nonintegral Q_z/Q_0 positions of the characteristic resonance peaks we observe indicate superlattice periodicities in molecular azimuthal orientations Ψ_j . These periodicities have been shown to be two, three, and four layers, respectively, in the SmC_A^* , $\text{SmC}_{\text{F11}}^*$, and $\text{SmC}_{\text{F12}}^*$ phases of the R-enantiomer 10OTBBB1M7 thiobenzoate compound, with a two-layer superlattice period also present in the SmC_A phase of the corresponding racemate. A temperature-dependent periodicity incommensurate with layer spacing was detected in the SmC_α^* phase window of 10OTBBB1M7.

We have shown that both the positions of the observed resonance peaks in 10OTBBB1M7 and their polarization states are in agreement with the predictions of the clock model describing the SmC^* variants. The model incorpo-

rates both a short clock pitch for Ψ_j corresponding to our observed superlattice periodicity, and a longer optical pitch due to the inherent chirality of the molecules. Our data also allow us to rule out the previously proposed Ising and bilayer models as candidates for describing the complete SmC^* variant series, and at the same time indicate important directions to pursue in future polarized resonant x-ray-scattering experiments.

We have also performed resonant x-ray-scattering studies upon the MHDDOPTCOB liquid-crystal compound containing a sulfur atom in a core thiophene ring. The results show that the atom containing the exploited resonance edge can be located in quite different rigid chemical substructures without diminishing our technique’s sensitivity to molecular orientation with respect to incident x-ray polarization. This reinforces the power of polarized resonant x-ray scattering for probing phases with orientational ordering that is undetectable by conventional methods. While polarized resonant x-ray scattering has been applied with success to materials in conventional crystalline phases [38], our results indicate that the technique will be critically important for soft condensed-matter studies as well.

To our knowledge, our results on the MHDDOPTCOB compound have provided the first observations of resonant satellite peaks originating from the optical pitch of the SmC^* phase, a periodicity that is also unobservable via conventional x-ray diffraction. We observed a characteristic four-layer superlattice in the ferrielectric temperature window for MHDDOPTCOB, indicating that the $\text{SmC}_{\text{F12}}^*$ structure previously found in 10OTBBB1M7 is not unique to one material, and may be of quite general occurrence. The resonance peaks detected in the SmC_A^* phase of MHDDOPTCOB also imply the same structure seen in the corresponding phase of 10OTBBB1M7.

ACKNOWLEDGMENTS

We would like to gratefully acknowledge M. Cepic, A. Fukuda, V. Lorman, B. Pansu, S. Pikin, and B. Zeks for detailed and thought-provoking discussions. We are grateful as well for many helpful conversations with S. Pankratz and P. Johnson. The experimental work reported here was supported in part by a National Science Foundation (NSF) grant. One of us (P.M.) would like to acknowledge support from the NSF and the University of Minnesota. Another of us (H.B.) acknowledges the support granted by the German national science foundation DFG. We thank S. Cheung, R. Greene, and T. Lenhard for their extensive technical assistance. The NSLS is operated by Brookhaven National Laboratory under Contract No. DE-AC02-76CH00016 with the U.S. Department of Energy, Office of Basic Energy Sciences.

-
- [1] A. D. L. Chandani, E. Gorecka, Y. Ouchi, H. Takezoe, and A. Fukuda, *Jpn. J. Appl. Phys., Part 2* **28**, L1265 (1989).
 [2] R. B. Meyer, L. Liebert, L. Strzelecki, and P. Keller, *J. Phys. (France) Lett.* **36**, L-69 (1975).
 [3] A. Fukuda, Y. Takanishi, T. Isozaki, K. Ishikawa, and H. Takezoe, *J. Mater. Chem.* **4**, 997 (1994); this review includes a

summary of SmC^* variant phases.

- [4] Y. Yamada, N. Yamamoto, K. Mori, K. Nakamura, T. Hagiwara, Y. Suzuki, I. Kawamura, H. Orihara, and Y. Ishibashi, *Jpn. J. Appl. Phys., Part 1* **29**, 1757 (1990).
 [5] M. Johnno, A. D. L. Chandani, J. Lee, Y. Ouchi, H. Takezoe, A. Fukuda, and K. Itoh, *Proc. Soc. Inf. Disp.* **31**, 129 (1990).

- [6] N. Yamamoto, N. Koshoubu, K. Mori, K. Nakamura, and Y. Yamada, *Ferroelectrics* **149**, 295 (1993).
- [7] K. Itoh, M. Kabe, K. Miyachi, Y. Takanishi, K. Ishikawa, H. Takezoe, and A. Fukuda, *J. Mater. Chem.* **7**, 407 (1997).
- [8] K. Hiraoka, T. Tsumita, Y. Sugiyama, K. Monzen, Y. Uematsu, and Y. Suzuki, *Jpn. J. Appl. Phys., Part 1* **36**, 6847 (1997).
- [9] I. Musevic, A. Rastegar, M. Cepic, B. Zeks, and M. Copic, *Phys. Rev. Lett.* **77**, 1769 (1996).
- [10] M. Skarabot, M. Cepic, B. Zeks, R. Blinc, G. Heppke, A. V. Kityk, and I. Musevic, *Phys. Rev. E* **58**, 575 (1998).
- [11] K. Ema, H. Yao, I. Kawamura, T. Chan, and C. W. Garland, *Phys. Rev. E* **47**, 1203 (1993).
- [12] H. T. Nguyen, J. C. Rouillon, P. Cluzeau, G. Sigaud, C. Destrade, and N. Isaert, *Liq. Cryst.* **17**, 571 (1994).
- [13] E. Gorecka, A. D. L. Chandani, Y. Ouchi, H. Takezoe, and A. Fukuda, *Jpn. J. Appl. Phys., Part 1* **29**, 131 (1990).
- [14] Ch. Bahr and D. Fliegner, *Phys. Rev. Lett.* **70**, 1842 (1993).
- [15] Y. Galerme and L. Liebert, *Phys. Rev. Lett.* **66**, 2891 (1991).
- [16] Y. Takanishi, K. Hiraoka, V. Agrawal, H. Takezoe, A. Fukuda, and M. Matsushita, *Jpn. J. Appl. Phys., Part 1* **30**, 2023 (1991).
- [17] Y. Takanishi, A. Ikeda, H. Takezoe, and A. Fukuda, *Phys. Rev. E* **51**, 400 (1995).
- [18] A herringbonelike, alternating orientation of molecules in SmC_A^* layers, with correspondingly antiparallel in-layer polarizations, was revealed by optical and ellipsometry work (Refs. [14], [15]).
- [19] P. Mach, R. Pindak, A.-M. Levelut, P. Barois, H. T. Nguyen, C. C. Huang, and L. Furenid, *Phys. Rev. Lett.* **81**, 1015 (1998).
- [20] M. Cepic and B. Zeks, *Mol. Cryst. Liq. Cryst. Sci. Technol., Sect. A* **263**, 61 (1995); V. L. Lorman, *ibid.* **262**, 437 (1995); S. A. Pikin, S. Hiller, and W. Haase, *ibid.* **262**, 425 (1995); A. Roy and N. Madhusudana, *Europhys. Lett.* **36**, 221 (1996).
- [21] A.-M. Levelut and B. Pansu, following paper, *Phys. Rev. E* **60**, 6803 (1999).
- [22] T. Isozaki, T. Fujikawa, H. Takezoe, A. Fukuda, T. Hagiwara, Y. Suzuki, and I. Kawamura, *Jpn. J. Appl. Phys., Part 1* **31**, 1435 (1992).
- [23] K. Hiraoka, Y. Takanishi, K. Sharp, H. Takezoe, and A. Fukuda, *Jpn. J. Appl. Phys., Part 2* **30**, L1819 (1991).
- [24] Physical properties of selected compounds from this series have been published elsewhere (Ref. [12]).
- [25] V. E. Dmitrienko, *Acta Crystallogr., Sect. A: Found. Crystallogr.* **39**, 29 (1983).
- [26] For examples of this effect in anomalous x-ray diffraction and absorption spectra studies on *crystalline* materials, see D. H. Templeton and L. K. Templeton, *Acta Crystallogr., Sect. A: Found. Crystallogr.* **42**, 478 (1986); L. K. Templeton and D. H. Templeton, *ibid.* **44**, 1045 (1988).
- [27] For film thicknesses of greater than roughly 15 layers, the films exhibit distinct coloring due to optical interference effects, making it possible to estimate their thickness. A discussion is given in E. B. Sirota, P. S. Pershan, L. B. Sorensen, and J. Collet, *Phys. Rev. A* **36**, 2890 (1987). The films studied in our experiment were approximately 250 layers thick.
- [28] The bulk phase sequence available does not distinguish between $\text{SmC}_{\text{F11}}^*$ or $\text{SmC}_{\text{F12}}^*$ for the nature of the ferroelectric temperature window of MHDDOPTCOB.
- [29] We determined this value for E_0 by using our standard fluorescence measurement technique on bulk MHDDOPTCOB; despite the very different position of the sulfur in MHDDOPTCOB as compared to 10OTBBB1M7, their resonance energies are in remarkable agreement.
- [30] The resonance origin of all the nonintegral Q_z/Q_0 peaks in 10OTBBB1M7 was individually confirmed by performing scans at energies other than the resonance value. The peaks disappear if x-ray energy is shifted by less than 1% from 2.475 keV (Ref. [19]), similar to what is seen for the MHDDOPTCOB compound in Fig.3.
- [31] 10OTBBB1M7 racemate shows the following phase sequence: isotropic, SmA, SmC, SmC_A , and crystal phases.
- [32] The FWHM of our system resolution function was found to be $1.6 \times 10^{-3} Q_0$.
- [33] The very small offset in the position of the $\text{SmC}_{\text{F12}}^*$ peaks from exact quarter-integer Q_0 values is most likely due to a slight change in layer spacing between the time these scans were acquired and the most recent previous layer thickness assignment based on a detailed scan of the (002) peak location. For reference, our confidence in the absolute Q_z assignments for observed peaks ($\pm 0.002 Q_0$) would correspond to approximately $\pm 0.13\%$ in layer spacing for this $\text{SmC}_{\text{F12}}^*$ phase, or equivalently a tilt angle variation of approximately $\pm 0.3^\circ$.
- [34] We have to date failed to observe a distinct x-ray signature corresponding to an ordinary SmC^* phase in the 10OTBBB1M7 material, although bulk measurements indicate that such a phase should be expected between SmC_α^* and $\text{SmC}_{\text{F12}}^*$ (Ref. [12]). However, the temperature window for the bulk SmC^* phase is quite narrow (only 1 K).
- [35] H. Orihari and Y. Ishibashi, *Jpn. J. Appl. Phys., Part 2* **29**, L115 (1990); B. Zeks and M. Cepic, *Liq. Cryst.* **14**, 445 (1993); V. L. Lorman, A. A. Bulbitch, and P. Toledano, *Phys. Rev. E* **49**, 1367 (1994).
- [36] This agrees with a previously reported value: V. Laux, N. Isaert, G. Joly, and H. T. Nguyen, *Liq. Cryst.* **26**, 361 (1999).
- [37] The SmC^* phase can be thought of as one in which the usually short clock pitch P_c has unwound to infinity ($\nu=\infty$), leaving just the optical pitch P_0 due to molecular chirality. For our $T = 86.2$ C MHDDOPTCOB data (Fig. 3), inserting the observed layer spacing of $d = 34.9 \text{ \AA}$ into Eq. (1) above yields a SmC^* optical pitch $P_0 = 2900 \text{ \AA}$. Considering a typical liquid-crystal refractive index of approximately 1.5, such a value would indicate a selective reflection of light of wavelength $\approx 0.45 \mu\text{m}$ from our sample, in agreement with the bright blue color of the film under crossed polarizers which we observed at this temperature.
- [38] Y. Murakami, J. P. Hill, D. Gibbs, M. Blume, I. Koyama, M. Tanaka, H. Kawata, T. Arima, Y. Tokura, K. Hirota, and Y. Endoh, *Phys. Rev. Lett.* **81**, 582 (1998).